International Journal of Rock Mechanics & Mining Sciences 53 (2012) 166–178

Contents lists available at SciVerse ScienceDirect

International Journal of Rock Mechanics & Mining Sciences

journal homepage: www.elsevier.com/locate/ijrmms

Integration of field characterisation, mine production and InSAR monitoring data to constrain and calibrate 3-D numerical modelling of block caving-induced subsidence

Kyu-Seok Woo [a,1,*], Erik Eberhardt [a], Bernhard Rabus [b], Doug Stead [c], Alex Vyazmensky [d,2]

[a] Geological Engineering, EOS, University of British Columbia, Vancouver, Canada
[b] MDA Systems, Ltd., Richmond, Canada
[c] Simon Fraser University, Burnaby, Canada
[d] Rio Tinto Copper Projects, Vancouver, Canada

ARTICLE INFO

Article history:
Received 11 April 2011
Received in revised form
23 March 2012
Accepted 3 May 2012
Available online 4 June 2012

Keywords:
Block caving
Subsidence
InSAR monitoring
3-D numerical analysis
Model calibration

ABSTRACT

Block caving often leads to significant ground deformations that if not properly assessed and accounted for may threaten the integrity and safety of overlying mine infrastructure. To mitigate this risk, sophisticated 3-D numerical modelling has been turned to as a means of predicting the extent and magnitudes of caving-induced surface subsidence. However, the complexity of the rock mass interactions involved, coupled with the uncertainty associated with geological heterogeneity, rock mass properties and in-situ stresses results in the need for models to be constrained and calibrated. Results are first presented here from a detailed 3-D back analysis of a caving-induced open pit mine slope failure, used to constrain the rock mass properties and far-field in-situ stresses derived from field characterisation data, as well as to bring understanding to the problem with respect to the cave-pit interactions. The "best fit" set of input properties obtained was then used for forward modelling of caving-induced subsidence for the period 2009–2010. Further calibration of this model was performed using high-resolution InSAR monitoring data. The close fit achieved between the predictive 3-D numerical model and InSAR data demonstrates the promise of InSAR as a means to calibrate sophisticated numerical models, and thereby contribute to managing block caving associated subsidence hazards.

© 2012 Elsevier Ltd. All rights reserved.

1. Introduction

The use of block caving to mine deep, massive, low grade orebodies is often favoured by the mining industry given its merits in terms of safety, tonnages produced and costs that can often compete with those of open pit operations. As an underground mass mining method, however, significant ground surface deformations often develop. If these are not properly assessed and accounted for, they may threaten the integrity and safety of overlying mine infrastructure. To better manage such risks, detailed engineering studies are undertaken to characterize the ground conditions and provide input for empirical and numerical design calculations.

Empirical relationships are generally used for preliminary scoping calculations, for example to estimate caving angles based on rock mass quality [1]. These do not explicitly account for the influence of stress–strain interactions and geological heterogeneity that may significantly affect the ground deformation profile. Instead, investigators have increasingly turned to advanced 2-D and 3-D numerical modelling to improve the assessment and understanding of block-caving subsidence dynamics and surface-underground interactions [2–8].

As in any modelling study, the results depend on the initial conditions and material properties assumed. These can vary greatly in accordance with the geological heterogeneity and variability encountered on site, with ranges of input properties being more likely than a single value. Furthermore, the numerous surface and underground interactions involved – both spatial and temporal – result in a complex 4-D problem that challenges even the most sophisticated numerical models.

The resulting model and parameter uncertainty necessitates that the models be constrained and calibrated in order to gain confidence in their output. This paper examines these issues based on detailed back and forward analyses of the Palabora block caving operation in South Africa. The first part of this paper focusses on the back analysis of a large 800 m high pit slope failure that occurred in response to block caving activities below the pit. This was used to constrain a 3-D finite-difference model against

* Corresponding author at: AMC Mining Consultants (Canada) Systems, Ltd., 200 Granville Street, Vancouver, British Columbia, Canada V6C 1S4. Tel.: +1 604 669 0044; fax: +1 604 669 1120.
E-mail addresses: Kwoo@amccounsultants.ca, kyuseokwoo@gmail.com (K.-S. Woo).
[1] Now at AMC Mining Consultants (Canada) Systems, Ltd.
[2] Now at Kazakhmys PLC, Almaty, Kazakhstan.

1365-1609/$ - see front matter © 2012 Elsevier Ltd. All rights reserved.
http://dx.doi.org/10.1016/j.ijrmms.2012.05.008

the range of rock mass strength values and in-situ stress ratios derived from field investigation data. The second part of this paper reports the use of these "best fit" input properties to forward model the caving-induced subsidence at Palabora for the period 2009–2010. High resolution satellite-based Interferometric Synthetic Aperture Radar (InSAR) data was used to further calibrate the 3-D numerical model developed. Together, the results presented demonstrate the promise of InSAR as a means to calibrate sophisticated 3-D subsidence models, improving our ability to assist mining companies to execute safe, economic and sustainable mining practices.

2. Palabora case history

The Palabora copper mine is a large, 30,000 t/day block cave operation located in the eastern half of Limpopo, South Africa's northern most province. Underground mining commenced in April 2001 after transitioning from an earlier open pit operation with target production being achieved in May 2005. The dimensions of the pit are approximately 800 m deep and 1650 to 1900 m in diameter, with slope angles ranging from 37° in the upper half of the pit to 58° in the lower, more competent lithologies. The block cave undercut level is approximately 1200 m below surface, 400 m below the pit floor (Fig. 1). The production level below the undercut consists of 20 cross-cuts spaced across a footprint 650 m long by approximately 250 m wide [9].

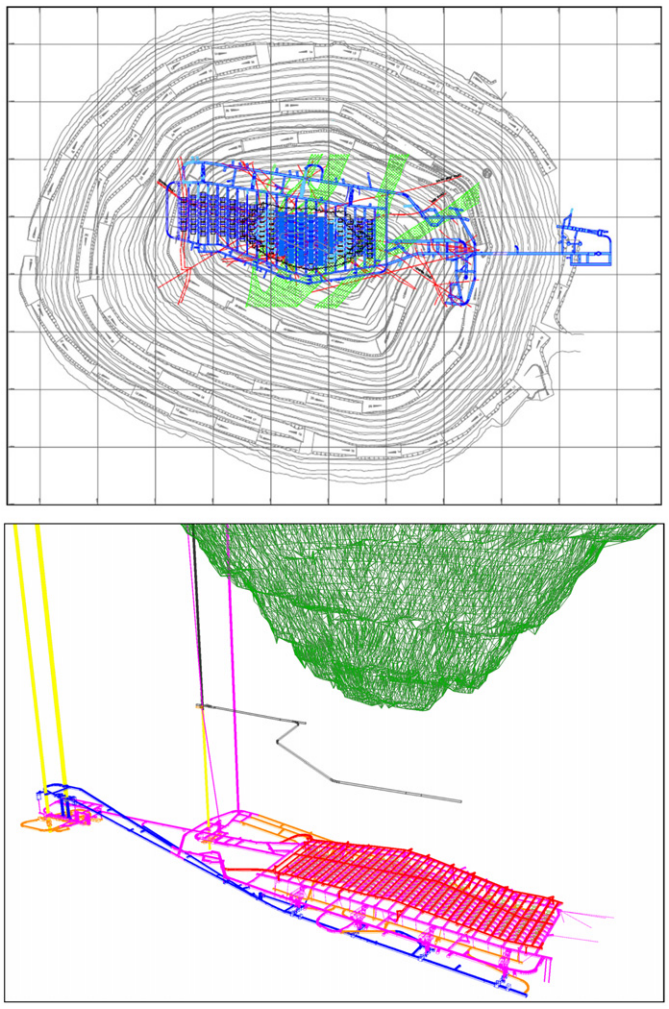

Fig. 1. Digital mine plans of the Palabora open pit and undercut geometries, showing their proximate location to one another. Modified after Ref. [9].

Fig. 2. Quickbird image of the northwest wall failure at Palabora.

Three years after the initiation of caving, cracking was observed in the northwest wall of the pit. These evolved over several months into major movements and eventually failure of the 800 m high pit wall shortly after breakthrough of the cave into the bottom of the pit (Fig. 2). The failure extended 300 m beyond the outer perimeter of the pit, affecting access and haul roads, tailings, water and power lines, water reservoirs and a railway line [9]. Fortunately, other critical mine infrastructure were not affected.

Moss et al. [9] remarked that the failure at Palabora revealed deficiencies in our understanding of cave–pit interactions. Subsequently, a number of studies were carried out applying sophisticated numerical modelling to back analyse the Palabora failure [4,6–8]. Brummer et al. [4] first examined the failure mechanism using the 3-D distinct element code 3DEC to model the influence and kinematic control of major geological structures. Their findings showed that the observed movements were potentially caused by wedges formed by pervasive joints that daylight into the cave region below the pit.

Another key study was that by Vyazmensky [7], who applied a hybrid finite-element/discrete-element modelling approach that simulates brittle fracturing within a network of non-persistent discontinuities. His work highlights the importance of joint set orientation on influencing the direction of cave propagation, as well as the importance of rock bridges and their incremental failure through cave–pit interactions leading to the progressive failure of the Palabora pit slope [8].

Although the preceding back analyses have made significant contributions to our understanding of the pit slope failure mechanism associated with block caving at Palabora, Moss et al. [9] also stress that given the level of up-front capital investment in a block cave, it is extremely important to develop reliable predictive tools. This emphasises the need for reliable, well constrained and calibrated forward analyses of block caving induced subsidence.

3. Model constraint and calibration through back analysis

3.1. Palabora 3-D model geometry

A detailed 3-D geological model was constructed integrating digital mine plans (Fig. 1) with mine geology data (Fig. 3).

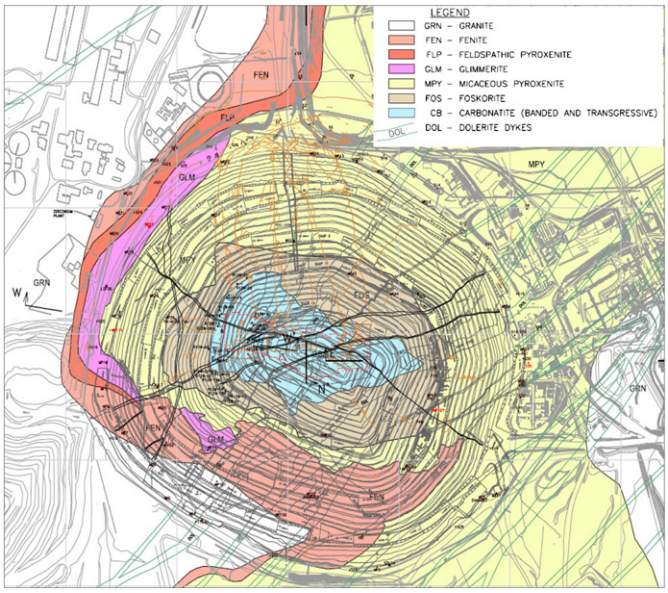

Fig. 3. Geological map for Palabora showing the key lithologies. After Ref. [11].

The Palabora Igneous Complex [10] consists of a succession of sub-vertical pipe-like bodies of alkaline and ultramafic rocks that have intruded into a host Archaean granite. The copper ore body occurs near the centre of the complex and is a composite vertical intrusion of micaceous pyroxenite subsequently intruded by foskerite and carbonatite. This body has then been cut by the emplacement of steeply dipping dolerite dykes.

The detailed geological model was used to develop a 3-D numerical model of the pit and undercut (Fig. 4) using the commercial finite difference code FLAC3D [12]. Implementation of the lithological units was limited in part by the resolution of the mesh; $15 \times 15 \times 15$ m elements were used to model the primary area of interest meaning that lithological domains with widths less than 15 m were not resolved. This includes the dolerite dykes. The external boundaries of the model measure 4000×4000 m in plan and 2000 m in depth. A gradational mesh with larger elements extending towards the outer model boundaries was employed. The 3-D mesh was iteratively tested and modified to limit numerical errors resulting from boundary effects and element shape and size.

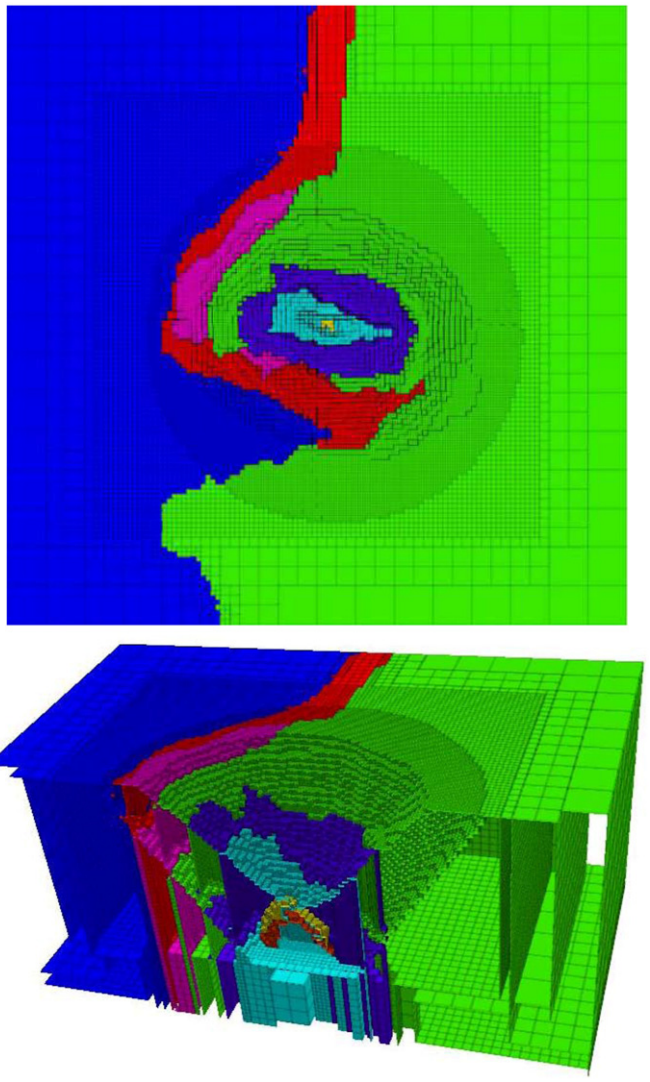

Fig. 4. FLAC3D model developed for back analysing the northwest wall failure (covering the period 2002–2005). Shown is the detailed geology built into the model in plan and 3-D perspective views. Model dimensions are 4000×4000 m in plan and 2000 m in depth.

3.2. Modelling of caving influence

The representation of the block cave and its development in the model is of prime importance given its direct relationship with the caving-induced deformations being modelled. This was implemented through an implicit approach where the geometry of the cave is built into the model, as opposed to explicitly modelling caving and cave propagation. The latter would have required considerable effort within the continuum framework to model the caving process accurately, alternating between small strain calculations applying a seismogenic/yield zone approach to model cave propagation and large strain calculations to model the corresponding ground deformations.

The implicit approach used here involves approximating the cave geometry at several different points in its development over time, and incrementally changing its properties from those of the ore body rocks to fragmented rock. This requires special consideration of the material properties of caved rock, and the redefinition of the induced stress state within the modelled cave material.

Adopting the implicit cave geometry approach, a procedure was developed for determining the cave geometry at any given

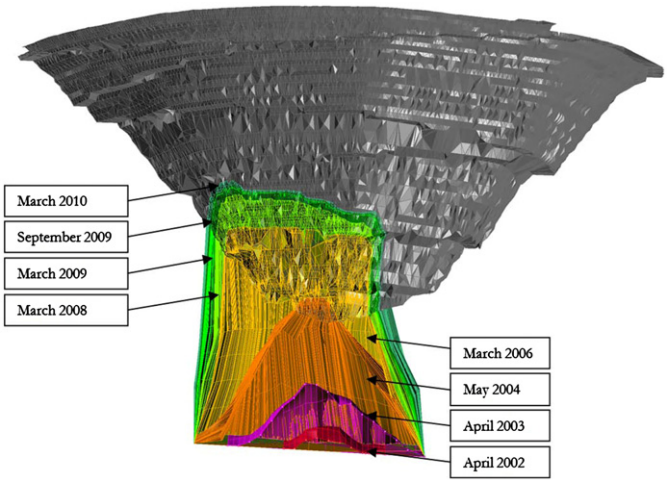

Fig. 5. Cave geometries for different time intervals implemented into the FLAC3D models.

point in time (Fig. 5). This involved extracting, for each time interval, the tonnages for each draw point from the mine production data, applying a 20% swell factor, calculating the cave height above each draw point, and comparing and modifying the resulting 3-D cave shape according to the mining-induced microseismic data for the same period.

3.3. Rock mass properties

The major lithological units represented in the FLAC3D model, and their rock mass characteristics, are summarised in Table 1. Rock mass properties were derived for each of these key lithologies (Fig. 4). This involved compiling data from mine geotechnical reports in which lab testing and rock mass characterisation data were reported. Because these reports span several different testing and field characterisation campaigns (over a period of more than 25 years), all data was carefully reviewed and evaluated to establish lower and upper bound values based on the minimum and maximum values reported, respectively (Table 2). This work was supplemented by field-based assessments made by the UBC-SFU team during fieldwork carried out at the mine in 2008. The rock mass descriptions and rock strengths provided are compiled from several modelling, laboratory testing, and field measurement sources. Not included in the model are the dolerite dykes, described as being composed of very strong rock, the jointing and several large fault zones.

From these, rock mass shear strength properties were estimated for use with a Mohr–Coulomb strain softening constitutive model. Most practitioners have more experience and therefore an intuitive feeling for the physical meanings of cohesion and friction on which the Mohr–Coulomb criterion is based. Accordingly Mohr–Coulomb rock mass shear strength properties for the use in the FLAC3D numerical modelling were derived through empirical procedures based on GSI, RMR and Q (e.g. Ref. [13]). Several empirical procedures exist to derive Mohr–Coulomb rock mass shear strength properties, one of the more commonly used being Hoek et al.'s [13] conversion of Hoek–Brown to Mohr–Coulomb achieved by fitting an average linear relationship to the non-linear Hoek–Brown envelope for a range of minor principal stress values with an upper bound of σ'_{3max}. Analytical relationships are provided for estimating σ'_{3max}, however these do not apply to block caving. Consequently, Hoek [14] recommends that caving analyses be carried out based either on Hoek–Brown or Mohr–Coulomb parameters, assessed independently, but not on the conversion of one to the other.

The applicability of these scaling relationships is noted here, but is also weighed against their required use: to simply provide an initial estimate of the rock mass shear strength properties, the values for which will then be varied and refined through the back analysis calibration exercise. Accordingly, the Hoek–Brown to Mohr–Coulomb conversion procedure was deemed adequate

Table 1
Major lithological units incorporated into the FLAC3D model and summary of their rock mass characteristics.

Unit	Geological description	Rock mass characteristics
Carbonatite	Igneous rock composed predominantly of carbonate minerals. Represented by two mineralogically similar units: a fine-grained Transgressive Carbonatite, which lacks significant foliation, and a medium- to coarse-grained Banded Carbonatite with vertical to steeply dipping foliation	Both units are relatively strong, with average UCS values of 120 MPa. They are described as being moderately fractured to massive (GSI 50–75) with mostly vertical jointing. Both are treated as one unit within the numerical model given their complex boundary contact and similar rock mass properties
Foskorite	Coarse-grained ultra-basic igneous rock composed of olivine, magnetite, apatite and phlogopite. It occurs on all walls as a broad zone between the Pyroxenite and the Carbonatite	Typically strong and competent with an average UCS of 90 MPa. This unit is described as being moderately to highly fractured (GSI 45–75) with mostly vertical jointing
Pyroxenite	Ultramafic igneous rock consisting essentially of minerals of the pyroxene group. Represented by two units: Feldspathic and Micaeous Pyroxenite. Feldspathic Pyroxenite occurs in limited quantities, primarily on the north and west sides of the pit. Micaceous Pyroxenite occupies a large portion of the north, west and east walls as well as a narrow band within the south wall	The UCS of Feldspathic pyroxenite is typically higher than the Micaceous, with average values of 100 and 85 MPa, respectively. These units are described as being highly fractured to massive (GSI 45–65) with mostly vertical jointing. Both are treated within the numerical model as one geomechanical unit
Glimmerite	An ultrabasic igneous rock, consisting almost wholly of essential dark mica, either phlogopite or biotite. Occurs in limited quantities on the western side and southwest corner of the pit	Highly variable strength, with an average UCS of 40 MPa. This unit is described as being highly fractured and sheared (GSI 35–50) with mostly vertical jointing. Glimmerite represents the weakest rockmass material present
Fenite	Na- and K-rich silicate rock developed through alteration of the Archaean granite contact. Fenite occupies a large portion of the South Wall and a narrow band behind the western and north-western pit crest	A hard, strong rock with an average UCS of 200 MPa. This unit is described as being moderately fractured (GSI 50–75) with mostly both vertical and horizontal jointing
Granite	Medium to coarse grained intrusive, felsic, igneous rock. The Archaean granite surrounds the complex and occupies a small section of the upper southwest pit wall	A hard, strong rock with an average UCS of 200 MPa. This unit was described as being relatively massive (GSI 70–80)

Table 2
Ranges of intact rock properties and rock mass rating values compiled from mine geotechnical reports and internal field assessments, and corresponding lower and upper bound rock mass properties derived.

Rock type	Intact rock properties				Rock mass characteristics & properties				
	Density (kg/m^3)	UCS (MPa)	E (GPa)	m_i	RMR	GSI	c_{rm} (MPa)	Φ_{rm} (°)	T_{rm} (MPa)
Carbonatite	2760–4720	75–172	30–58	15–17	60–80	50–75	3–8	40–58	0.1–1.5
Foskorite	2850–4420	26–150	40	17	56–75	45–75	2–7	30–55	0.02–1.3
Pyroxenite	2800–3240	39–136	15–38	15–17	54–70	45–65	2–5	30–54	0.04–0.6
Glimmerite	3100	37	6	17	50–55	35–50	1–3	25–34	0.01–0.05
Fenite	2610–2730	133–340	10	15–17	57–75	50–75	3–10	44–58	0.2–2.9
Granite	3100	200–300	31	32–33	75	70–80	6–11	55–63	0.5–2.1

UCS=Uniaxial Compressive Strength; E=Young's modulus; m_i=Hoek–Brown intact rock parameter; RMR=Rock Mass Rating; GSI=Geological Strength Index; c_{rm}=rock mass cohesion; Φ_{rm}=rock mass friction angle; T_{rm}=rock mass tensile strength.

and a σ'_{3max} value of 10 MPa was estimated for the conversion based on preliminary modelling of the stresses that develop between the cave and foot of the pit slopes. Table 2 reports the corresponding ranges of equivalent rock mass cohesion and friction angle values for the lower and upper bound values established for each rock mass unit represented in the FLAC3D model. These are in general agreement with values used in previous mine modelling studies. The lower- and upper-bound values were subsequently tested through a parametric analysis using the FLAC3D model to test the sensitivity of the modelled response to the material properties used.

3.4. In-situ stresses

Data for the in-situ stress boundary conditions were compiled based on regional stresses reported in the published literature and mine specific in-situ stress studies. Regional stress data reported in the World Stress Map database [15] and those in a study of South African mining areas [16] suggest that stress ratios in the region fall somewhere between 0.5 and 1.5 for the major horizontal to vertical stress ratio, and 0.5–1.0 for the minor horizontal to vertical stress ratio. These ranges bracket values obtained from in-situ stress measurements at Palabora [17–19], where investigations in 1992 and 1999 reported ratios ranging from 0.5 to 1.2 (Table 3). The variability seen in Table 3 is not uncommon for in-situ stress measurements, and may be due to local effects caused by major faults and/or geological heterogeneity.

A number of reports presenting results from numerical modelling for Palabora were further reviewed to see how the in-situ stress boundary conditions were treated for different aspects of the pit and cave designs (Table 4). Early studies assumed an in-situ stress ratio K_o of 1.0 [20], or assumed K_o to be 1.5–2.0 in the upper 200 m of the pit, decreasing linearly to about 1.1 at a depth of 2000 m [21]. More recently, numerical analyses have used a K_o varying between 1.5 and 2.0 based on findings from the Mass Mining Technology (MMT) project of the International Caving Study.

Based on this review, several different in-situ stress assumptions were tested in step with the model calibration for the best fit set of rock mass properties.

Table 3
Results from Palabora in-situ stress studies and measurement campaigns.

Year [reference]	Method	Stresses determined
1991 [22]	Back analysis	$\sigma_{NS}=2.0\sigma_V$ $\sigma_{EW}=1.5\sigma_V$
1992 [17]	Borehole slotter	$\sigma_{NS}=0.65\sigma_V$ $\sigma_{EW}=0.51\sigma_V$
1992 [18]	CSIR triaxial	$\sigma_{NS}=\sigma_V$ $\sigma_{EW}=0.97\sigma_V$
1999 [19]	CSIRO 12	$\sigma_1=46$ MPa (16°/323°) $\sigma_2=38$ MPa (73°/152°) $\sigma_3=36$ MPa (4°/051°)

Table 4
Horizontal to vertical in-situ stress ratios (K_o) used in different numerical modelling studies for Palabora.

Year	Method	K_o	Notes
1991	FLAC	1.0	Assumed for model calibration
1991	UDEC	1.5–2.0	Assumed
1995	FLAC3D	$\sigma_{NS}=1$ $\sigma_{EW}=0.97$	Based on 1992 measurements (Table 2)
1998	UDEC	1.0	Based on 1997 geotechnical review
1999	UDEC	1.2	Based on 1999 measurements (Table 2)
2000a	UDEC	1.0	Calibrated and back analysed using monitoring data for East Wall
2000b	UDEC	0.5–1.2	Based on 1992 and 1999 measurements (Table 2).
2004	3DEC	1.0	Based on modelling report.
2005	3DEC	$\sigma_{NS}=1$ $\sigma_{EW}=1$	Based on 1992 measurements (Table 2).
2008	FLAC3D	$\sigma_{NS}=2.0$ $\sigma_{EW}=1.5$	Based on MMT project results.
2009	FLAC3D	$\sigma_{NS}=1.5$ $\sigma_{EW}=2.0$	Based on MMT project results

3.5. Back analysis and model calibration

FLAC3D modelling of the 2005 northwest wall failure was carried out to back analyse and constrain the material properties

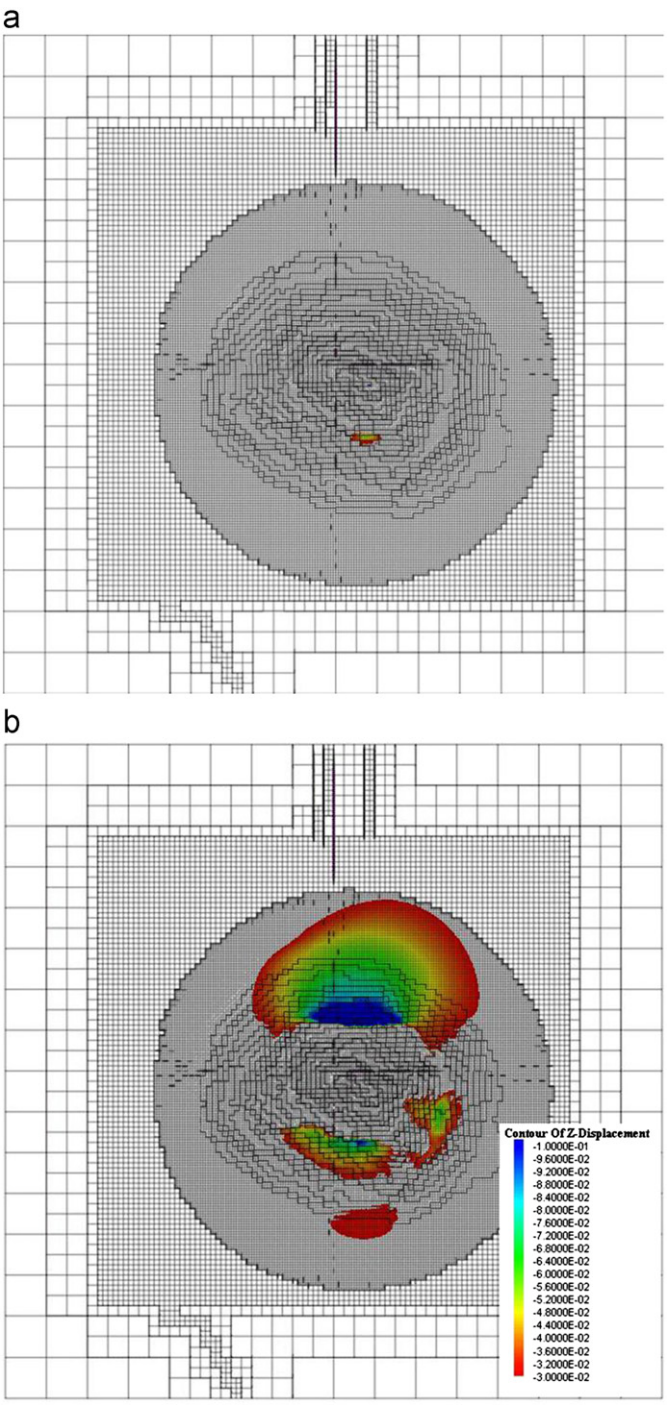

Fig. 6. Back analysis comparing caving-induced displacements assuming: (a) average, and (b) lower bound rock mass properties, based on the input ranges compiled in Table 1. Displacements are reported in metres.

and in-situ stresses to be used for subsequent forward modelling. Cave–pit interactions were modelled starting from the time of initial underground production in 2002 to the time of failure in 2005 in one year increments (Fig. 5). Full implementation of the caving simulation involved first initialising the stresses in the ore zone (i.e. calculated according to the depth of the host rock and acting horizontal in-situ stresses), and then modelling the advancement of the cave by changing the material properties of the ore to those of the caved rock in step with the upward propagation of the cave. A key step in this process is that the initialised stresses in the elements representing the caved material must be reset with each modelled advance of the cave to correspond with the self-weight of the caved rock and not the initial tectonic stresses.

Average rock mass properties and in-situ stress ratios from the ranges compiled in Tables 1 and 2, respectively, were tested and then varied depending on the closeness of the fit achieved between the modelled displacements and outline of the northwest wall failure. Several limitations in the modelling approach applied here must be noted. First, the presence of both meso-scale jointing in the northwest wall and major faults in its proximity would have played a significant role in the caving-induced slope failure process. These are not considered in the FLAC3D continuum representation of the slope. The results are also limited by the minimum element size, which influences the ability for a failure surface in the model to localise and develop. Due to these limitations, it is not possible to explicitly model the pit wall failure that occurred. Instead, the comparative analysis carried out relied on the distribution of caving-induced displacements, specifically those arising from strain softening, as the measure to compare the different back analysis model runs.

Results from the back analysis clearly showed a varied response for the different rock mass properties tested. Fig. 6 compares the caving-induced displacements modelled assuming a set of average rock mass properties (Fig. 6a) and those assuming the lower bound properties (Fig. 6b). The latter shows increased displacements in the northwest wall of the pit that approximately coincide with the northwest wall failure. Table 5 reports the calibrated rock mass properties judged as providing the best fit

Table 5
Back-analysed FLAC3D rock mass properties providing the best fit to the observed outline of the northwest wall failure. K and G denote the bulk and shear modulus, respectively, as derived from estimates of the rock mass Young's modulus and Poisson's ratio.

Rock Type	Elastic Properties			Rock Mass Strength Properties			
	Density (kg/m^3)	K (GPa)	G (GPa)	c_{rm} (MPa)	Φ_{rm} (°)	T_{rm} (MPa)	ε_p (–)
Carbonatite	3100	8	4	2.5	40	0.15	–
Foskorite	3100	4	2	2.5	35	0.1	–
Pyroxenite	3100	4	2	2	30	0.1	0.01
Glimmerite	3100	1	0.5	1.5	25	0.01	0.005
Fenite	3100	16	10	5	55	0.4	–
Granite	3100	20	12	6	55	0.65	–
Caved Rock	2300	0.2	0.1	–	–	–	–

K=bulk modulus; G=shear modulus; c_{rm}=rock mass cohesion; Φ_{rm}=rock mass friction angle T_{rm}=rock mass tensile strength; ε_p=plastic strain threshold for material strain softening (75%–90% reduction in strength).

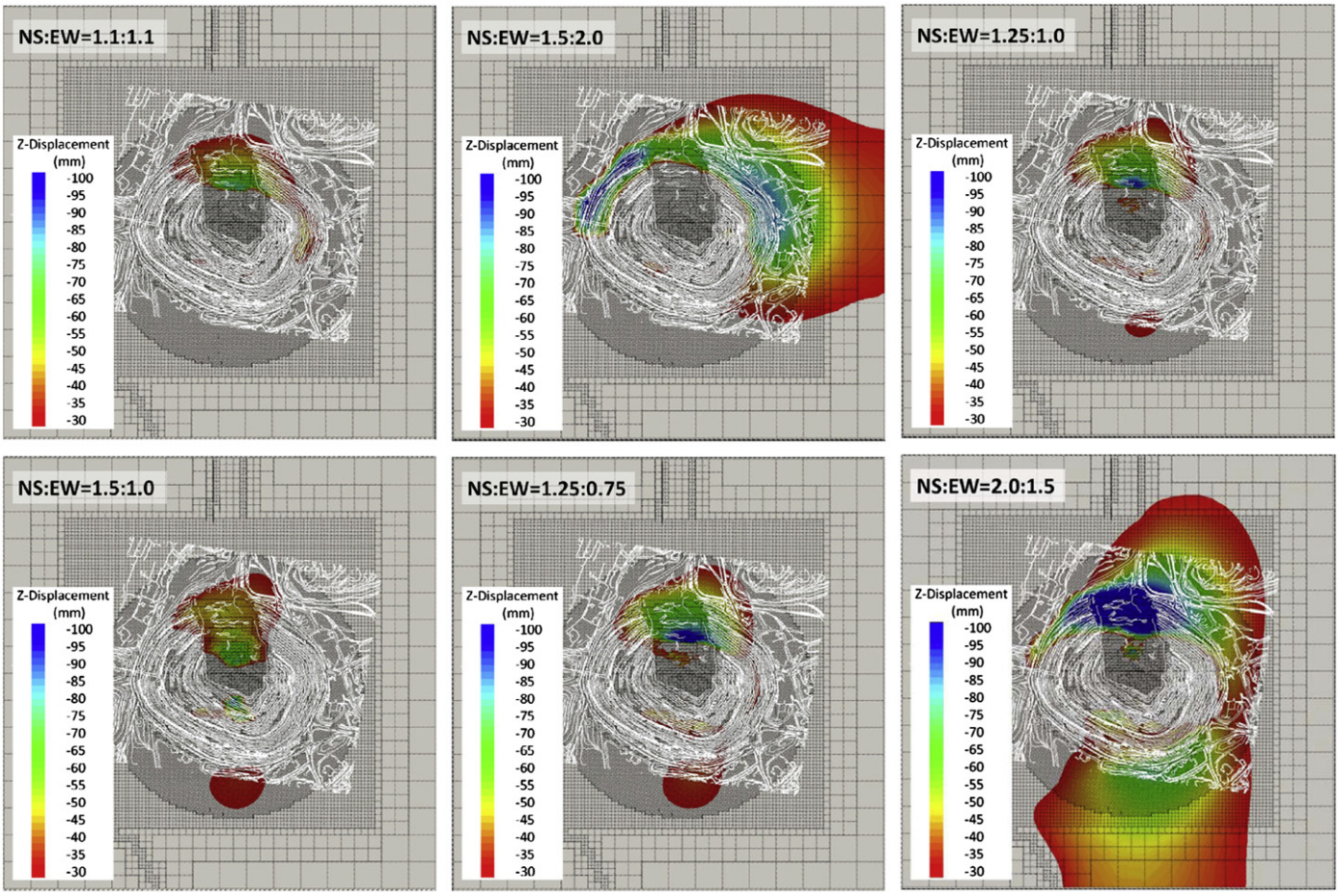

Fig. 7. FLAC3D results for several different in-situ stress assumptions. Superimposed are the contours outlining the northwest wall failure. Displacements are reported in metres.

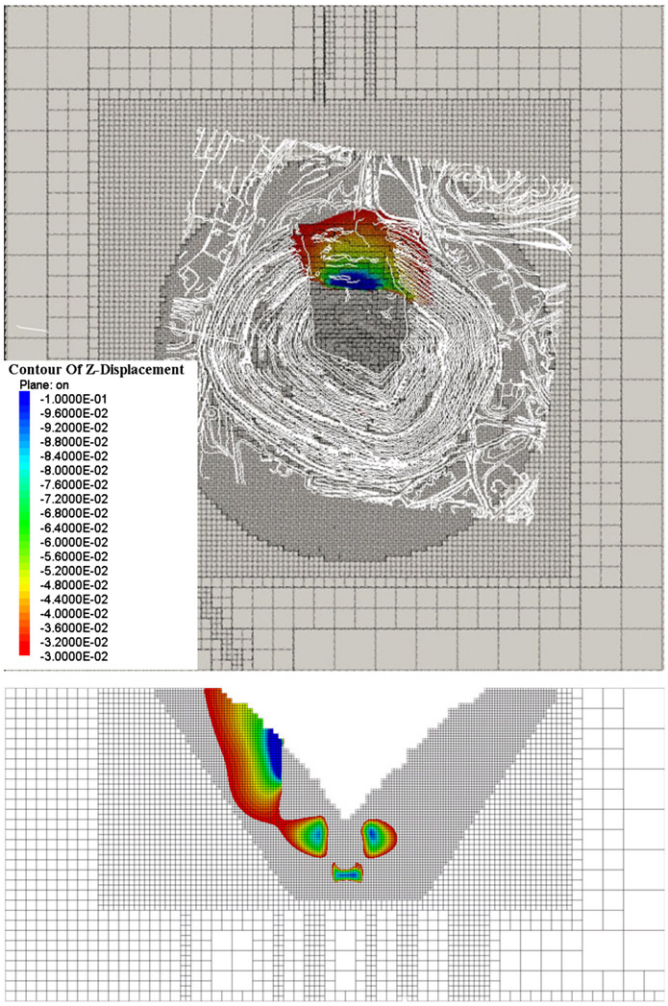

Fig. 8. Best fit FLAC3D model comparing modelled vertical displacements (greater than 3 cm) to the DEM outline of the North wall failure, in plan and along a North–South section through the centre of the northwest wall failure. NS and EW horizontal stresses are assumed to be equal to the vertical stresses ($K_o=1$). Displacements are reported in metres.

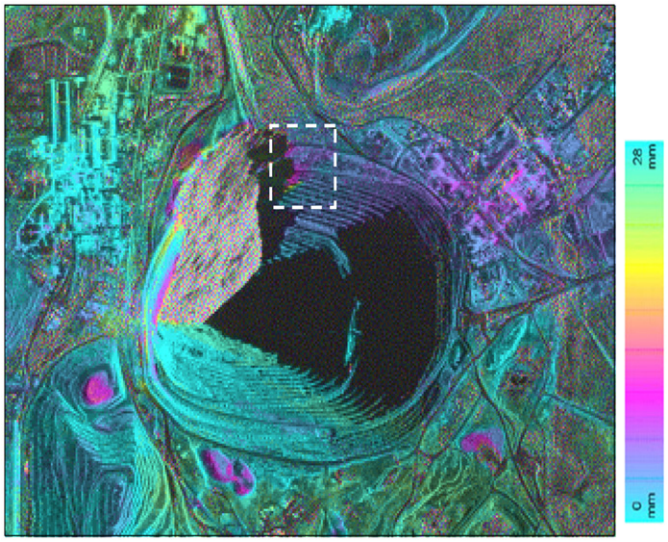

Fig. 9. RADARSAT-1 data for Palabora recorded for the two-year period following the 2005 northwest wall failure. The area highlighted by the white dashed box coincides with the extent of modelled displacements (greater than 3 cm) shown in Fig. 8.

for the back analysed northwest wall failure. These include testing of different strain softening thresholds at which strength degradation through brittle fracturing would begin (correlating induced plastic strains with reduced post-peak rock mass strengths). Results using the Mohr–Coulomb strain softening constitutive model produced significantly improved results over models solved assuming a simpler Mohr–Coulomb elasto-plastic constitutive model. Model calibration suggested that the influence of strain softening was most important for the pyroxenite and glimmerite units.

Also included in Table 5 are the material properties assumed for the caved rock. As the material responsible for the relaxation and deformation of the surrounding rock, it was found to have a significant influence on the magnitude of the modelled displacements. A detailed search of the literature proved unsuccessful in finding values for caved rock; several papers were found reporting values for broken rock as used in the construction of rockfill dams and for mine backfill and these were used as an initial starting point for the back analysis. However, these required additional calibration. To avoid numerical errors related to severe mesh distortion, the caved rock material was modelled as an elastic material, using reduced elastic properties to account for

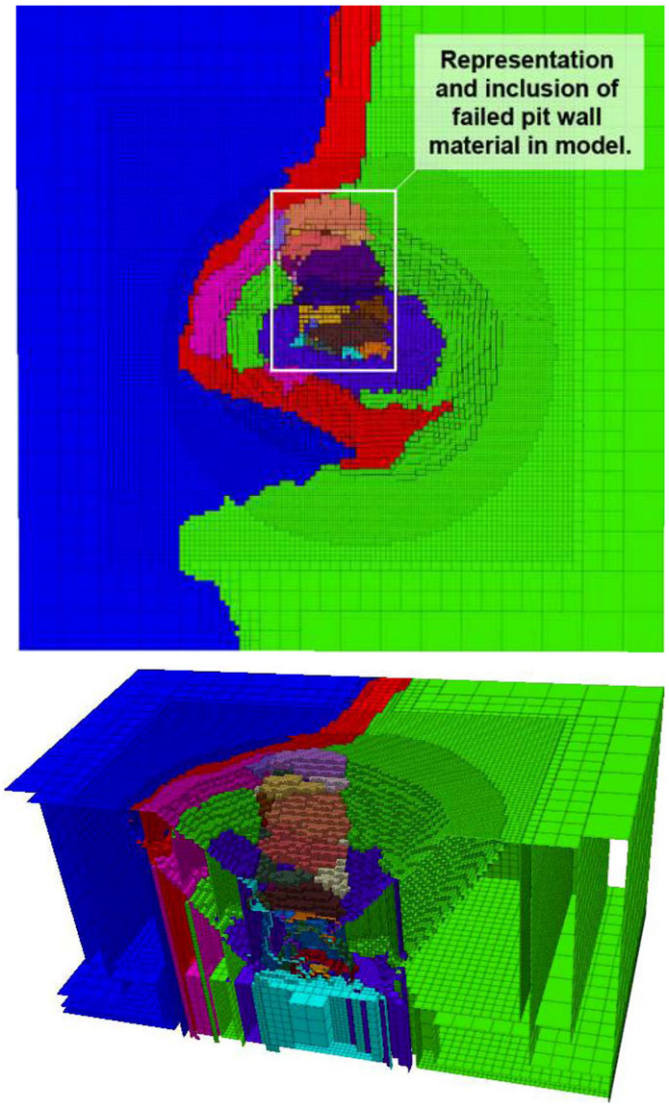

Fig. 10. Modified model geometry for forward modelling of caving-induced ground deformations for the period 2009–2010.

the reduced deformation modulus that would be expected for caved rock, as well as allowances for the presence of a small air gap.

Model calibration of the best-fit material properties was carried out in step with calibration of the assumed far-field in-situ stress boundary condition (Fig. 7). These showed that a uniform stress field where the NS and EW horizontal stresses equal the vertical stresses (i.e. $K_o=1$) provided the best fit to the outline of the northwest wall failure (Fig. 8). This stress field is in agreement with those in the World Stress Map database [15], those reported by Stacey and Wesseloo [16] and values reported in Tables 3 and 4. The contours in Fig. 8 adopt a vertical displacement cut-off of 3 cm, which is the National Coal Board's minimum threshold [22] for damage to surface infrastructure and an approximate indicator for the appearance of surface fractures (i.e. brittle fracturing of the rock mass). Given the continuum treatment of the problem, the closeness of the fit achieved suggests that the spatial positioning of the undercut beneath the pit but also partly beneath the north wall (see plan view projection in Fig. 1) was a key factor influencing the northwest wall failure. The 3-D model results clearly show that the interaction between the developing cave and open pit above was more pronounced for the northwest wall than any other area of the pit. These directed the cave towards the north where it undermined the toe of the slope eventually resulting in failure.

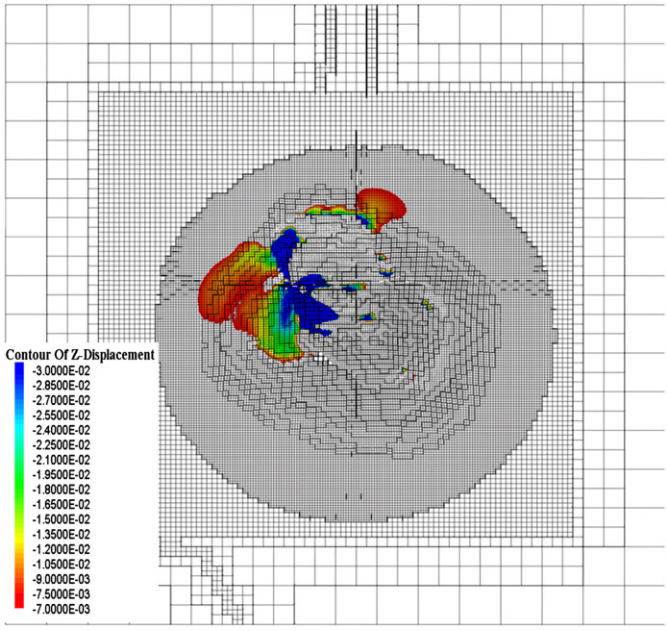

Fig. 11. FLAC3D forward modelling results showing the caving-induced vertical displacements for the period March 2009–March 2010 in plan view. Displacements are reported in metres.

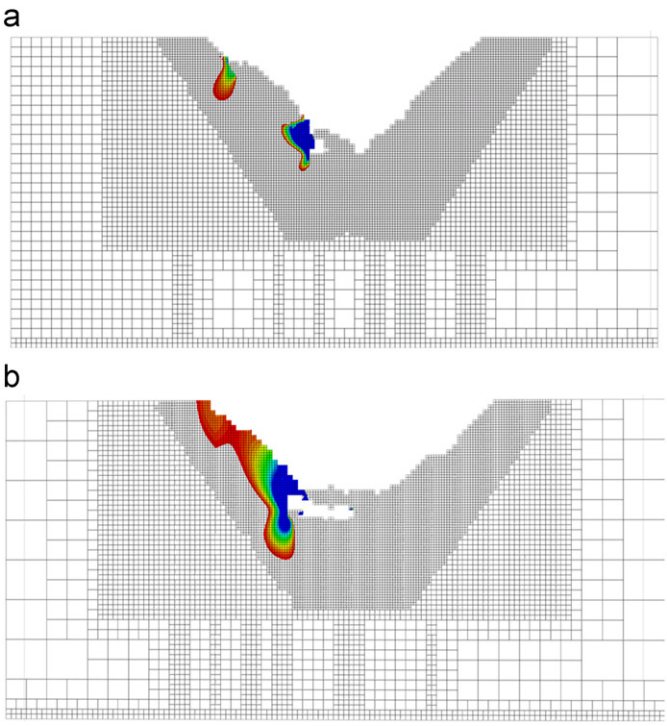

Fig. 12. FLAC3D forward modelling results showing the caving-induced vertical displacements for the period March 2009–March 2010: (a) N–S section, and (b) E–W section. Displacements are reported in metres.

4. InSAR monitoring as a means to constrain modelled displacements

Space-borne Synthetic Aperture Radar (SAR) involves the use of satellite-based microwave radar to remotely observe characteristics

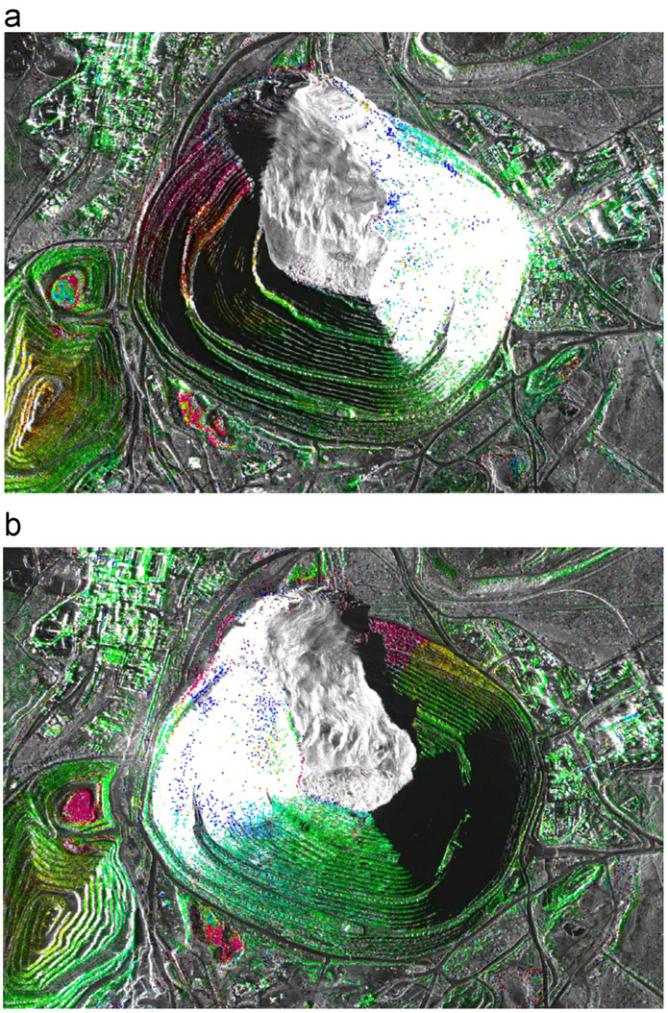

Fig. 13. RADARSAT-2 data for Palabora for the period March 2009–March 2010, showing: (a) ascending, and (b) descending InSAR measured vertical displacements. Points colour-coded with respect to downward movements are, Red: 20–40 mm, Yellow: 10–20 mm, Green: 0–10 mm. (For interpretation of the references to colour in this figure legend, the reader is referred to the web version of this article.)

of ground terrain. With repeated orbits and image capture (referred to as stacks), Interferometric SAR (InSAR) data can be processed to resolve 3-D information of surface deformations by analysing differences in the phase between waves being transmitted and received by the satellite [23]. Ground deformations can be detected on the scale of centimetres to millimetres for a surface area resolution of several square metres using these techniques. This ability to detect shape changes in a surface area with significant resolution provides a means to monitor mining-induced differential strains, including small strain ($<1\%$), that develop across an irregular surface topography.

Inspection of the results in Fig. 8 shows that the modelled displacement field extends to the east of the northwest wall failure. Although this at first may appear to suggest a minor mismatch between the model and observed extent of failure, subsequent integration with RADARSAT-1 data shows excellent agreement. Fig. 9 shows the InSAR measured displacements from the analysis of RADARSAT-1 images (8 m surface area resolution) for Palabora recorded for the two-year period following the 2005 northwest wall failure. The data shows that most of the measured displacements are concentrated along the north wall, especially towards the east along its crest. These would appear to be related to the instability of the pit wall in response to the cave breakthrough. Behind the pit rim and around the mine area in general, little subsidence is detected during this period. Comparing these displacements to those modelled in Fig. 8, both the areas of extent and magnitude of displacement are in close agreement. This provides an additional degree of confidence in carrying the back analysed input values forward for subsequent analysis of the current state of caving-induced subsidence.

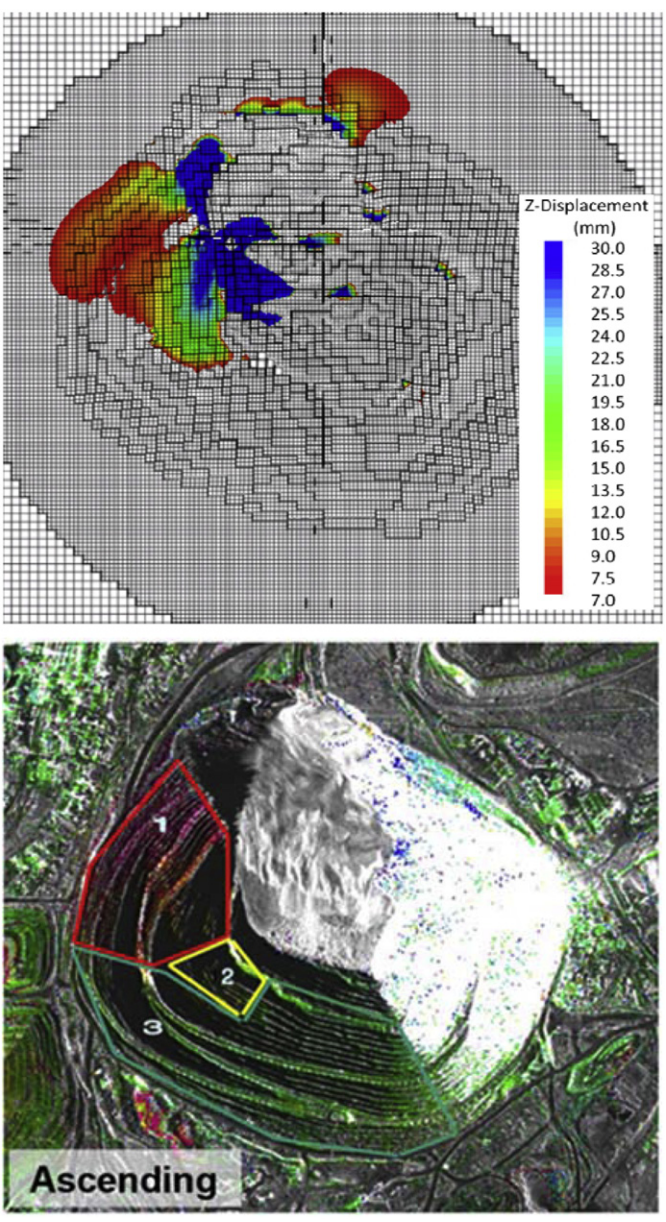

Fig. 14. Side-by-side comparison of FLAC3D modelling results with the ascending RADARSAT-2 data for the period March 2009 to March 2010. Downward subsidence magnitudes for the zoned regions correspond to: (1) 20–40 mm, (2) 10–20 mm, (3) 0–10 mm, and (4) shadow.

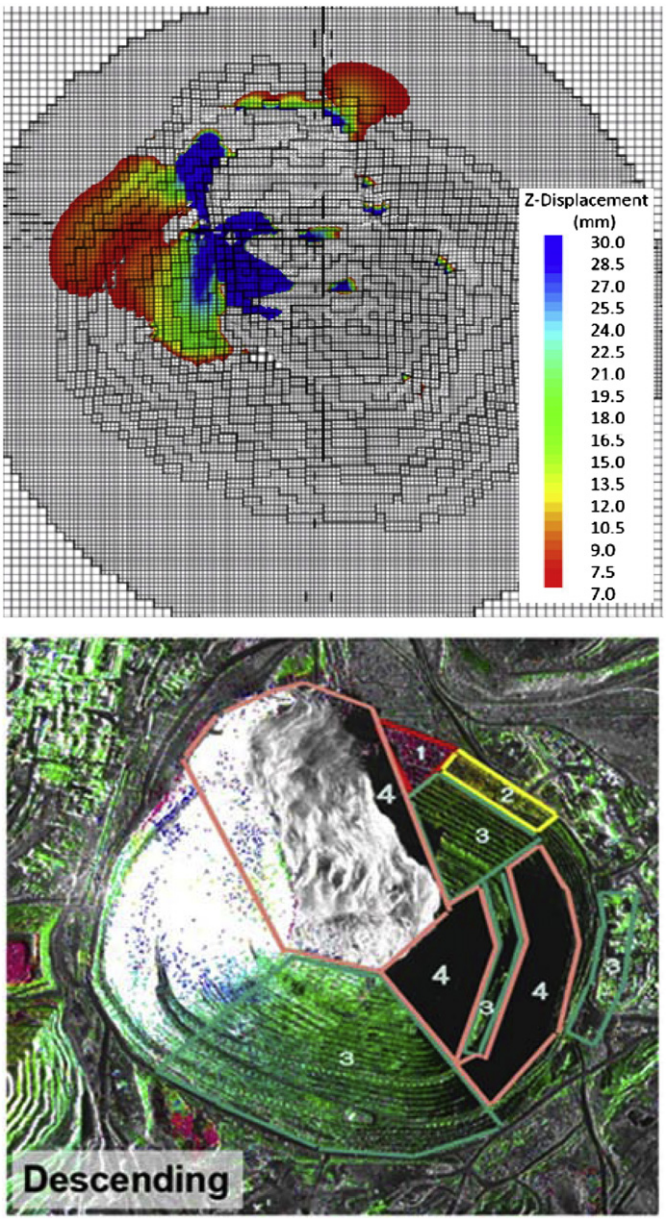

Fig. 15. Side-by-side comparison of FLAC3D modelling results with the descending RADARSAT-2 data for the period March 2009 to March 2010. Downward subsidence magnitudes for the zoned regions correspond to: (1) 20–40 mm, (2) 10–20 mm, (3) 0–10 mm, and (4) shadow.

5. Forward-modelling of caving-induced displacements (2009–2010)

5.1. Modifications to model geometry

The back analysis of the 2005 pit slope failure provided an important initial step in calibrating and constraining the FLAC3D subsidence model. However, the failure also represents a major change in the 3-D geometry of the mine model, including a localised deviation of the cave. These were accounted for in a modified 3-D model directed towards a forward analysis of caving-induced ground deformations for the period March 2009 to March 2010. Built into the model were the changing cave geometries for 2006–2010 (Fig. 5) together with the presence of the pit wall failure debris (Fig. 10). Thus, this modified model represents a continuation of the back analysis model incorporating the influence of the northwest wall failure.

The pit wall failure debris was assigned the same properties as the caved material (i.e. broken rock). In addition, the stress conditions in the failed zone were reassigned to represent those of the collapsed ground (i.e. gravity loading instead of the locked in $K_o=1$ in-situ stress condition used throughout the rest of the model). The presence of the failure debris also required special consideration in the construction and implementation of the post-failure cave geometries. A significant amount of slide debris sits above and on top of the pit floor bottom where the cave has broken through. Moss et al. [9] estimate the failure to be approximately 100 million tonnes and note that the potential exists for the slide/waste material to move at a faster rate than the ore rock within the cave as the cave is pulled due to differences in block size between the two (i.e. mechanical sieving). Thus, the production data used to project the changing volume of the cave after 2005 would likely include both caved rock (associated with the changing cave geometry) and slide debris entering the cave (not associated with the changing cave

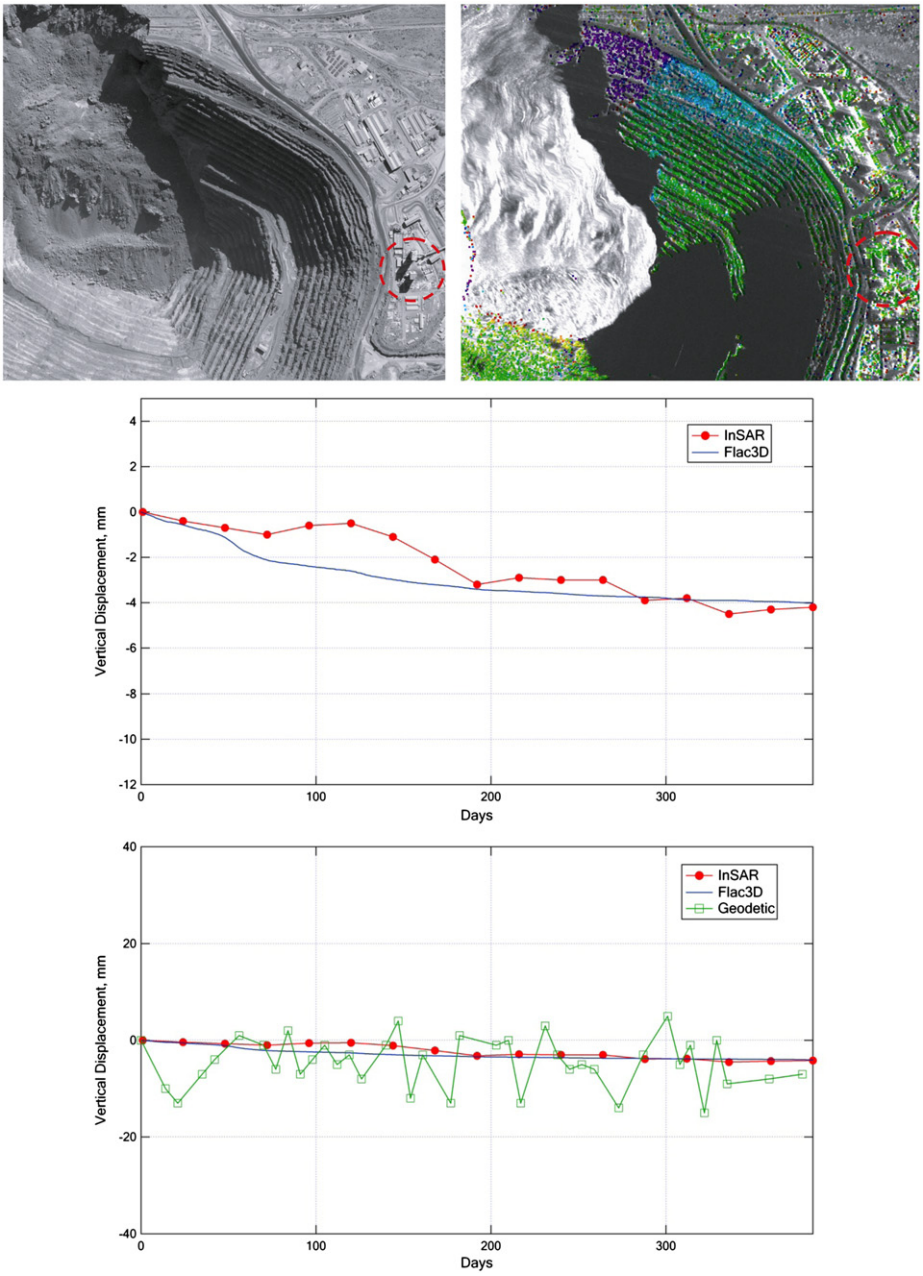

Fig. 16. Comparison of FLAC3D modelled and InSAR and mine geodetic measured vertical displacements between March 2009 and March 2010, for a history point/survey prism located near the main access shaft.

geometry). To correct for this, Digital Terrain Models (DTMs) and QuickBird satellite images for different periods between 2005 and 2009 were compared to approximate changes in volume of the rockslide material on surface and therefore that entering the cave. This analysis indicated that it is unlikely that debris was entering the cave prior to January 2006. Subsequent to this, however, an average volume of 2 million m^3 per year was resolved as entering the cave and was corrected for in generating the cave geometries. The caving intervals analysed include: March 2006, March 2008, March 2009, September 2009, and March 2010, where the last three intervals coincide with the beginning, mid-point and end of targeted RADARSAT-2 SAR data aquisitions carried out as part of this study.

5.2. RADARSAT-2 deformation monitoring

Through a partnership between the Canadian Space Agency, MDA Systems, the University of British Columbia and Simon Fraser University, targeted RADARSAT-2 data was collected to monitor mining-induced ground deformations at several open pit mine sites, including Palabora. Launched in December 2007, RADARSAT-2 is Canada's second-generation commercial SAR satellite, capable of providing surface area resolutions approaching 2×2 m. Together with improvements in data processing and inversion of the phase components (atmosphere, height error and displacement corrections), significant gains have been made in the robustness of the InSAR solution [24].

RADARSAT-2 data was collected for Palabora during the period March 2009 to March 2010, in 28 d intervals. The images were taken in ascending as well as descending modes. The processed InSAR deformations were then used to compare with the results from the FLAC3D forward modelling results.

5.3. FLAC3D forward modelling results and comparison with InSAR data

Figs. 11 and 12 show the FLAC3D forward modelling results for the caving-induced displacements for Palabora between March 2009 and March 2010. These predict total displacements on the

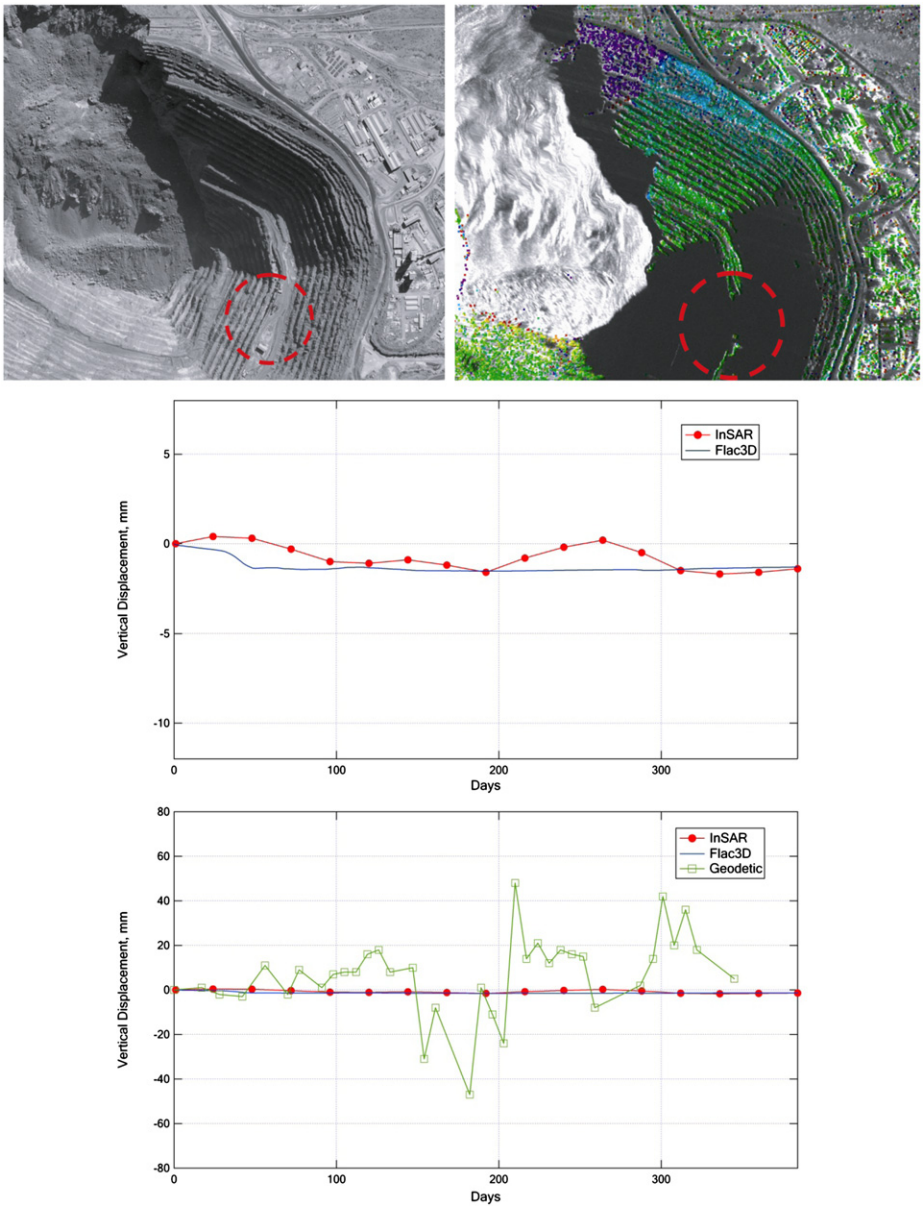

Fig. 17. Comparison of FLAC3D modelled and InSAR and mine geodetic measured vertical displacements between March 2009 and March 2010, for a history point/survey prism located near the ventilation shaft.

order of 5–15 mm along parts of the upper pit and crest, and 15–30 mm just above the bottom of the pit. Fig. 12 shows that the cave interaction with surface will have the greatest influence on the west pit wall with minor movement of the north wall. Fig. 13 shows the ascending and descending InSAR data for the same period. These show that most of the displacements (20–40 mm) correspond to ongoing activity to the east of the 2005 northwest wall failure (primarily near the crest) and to the west extending across half of the west wall. Otherwise, displacements are less than 10 mm for this time period along the east and south pit walls.

Figs. 14 and 15 present the side-by-side comparison of the FLAC3D results and corresponding ascending and descending InSAR images for the 2009–2010 data gathering period. Using the input properties derived from the back analysis, close agreement was achieved with respect to the spatial extent of the displacements. However, the displacement magnitudes predicted by the FLAC3D model are approximately 20% lower than those seen in the InSAR data. A better fit of the measured displacement magnitudes was subsequently achieved through minor calibration of the model in the form of decreasing the plastic strain threshold for strain softening for the pyroxenite from 0.01 to 0.005. Further comparisons of the calibrated FLAC3D subsidence model and the InSAR measured vertical displacements are shown for several targeted areas around the open pit, including the main access shaft (Fig. 16), the ventilation shaft (Fig. 17) and the crest above the west wall (Fig. 18). Also included are the vertical displacements calculated from the geodetic monitoring data, which show very good agreement.

The subsidence predicted by the FLAC3D model for the period of 2009–2010 closely fits the InSAR measurements during the same period, confirming the accuracy and reliability of the calibrated FLAC3D prediction. As for the geodetic data, the geodetic measurements show more variability in the subsidence rate than the InSAR measurements. Geodetic data are direct measurements taken on site

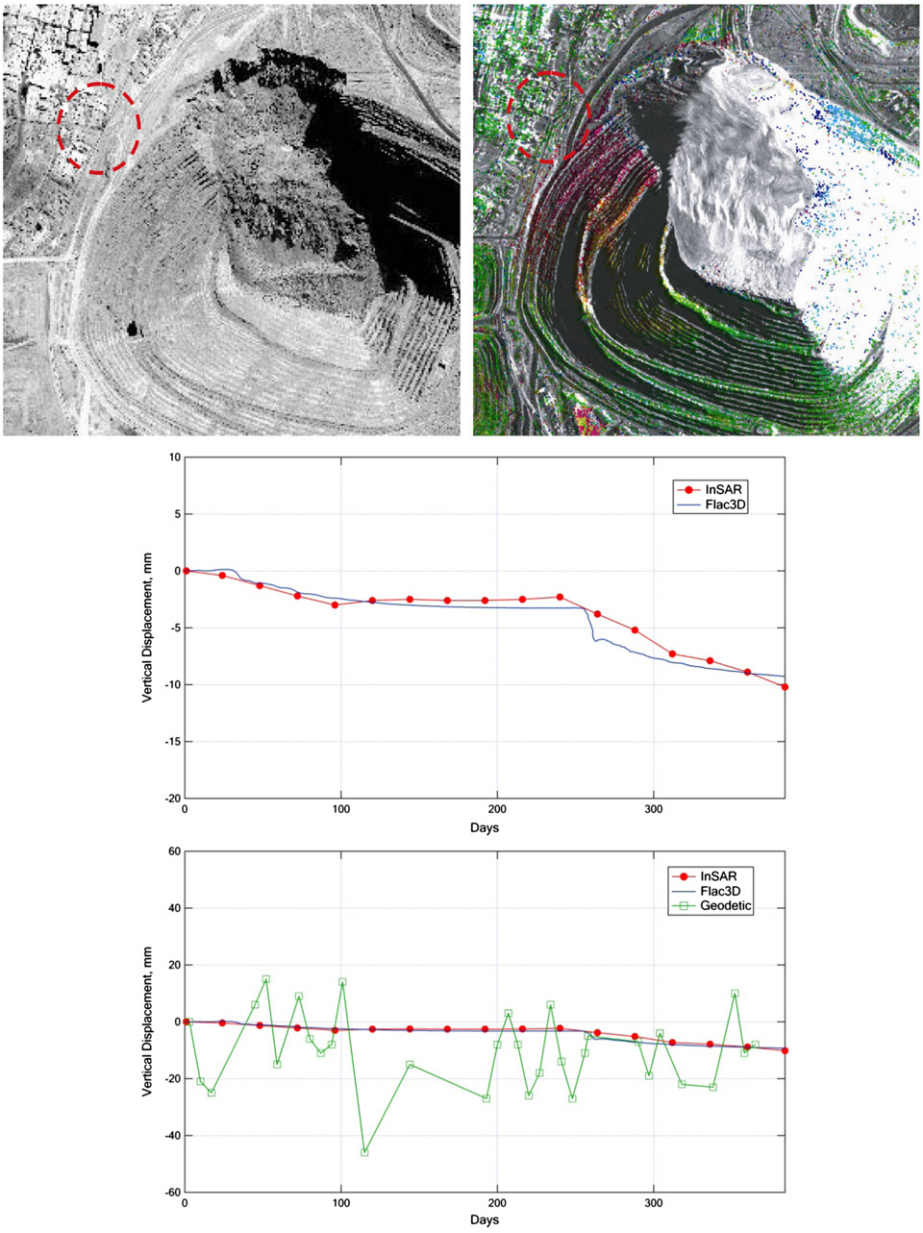

Fig. 18. Comparison of FLAC3D modelled and InSAR and mine geodetic measured vertical displacements between March 2009 and March 2010, for a history point/survey prism located above the crest of the west wall.

and thus presumed to be reliable. However, there are several potential deficiencies: geodetic data are not necessarily collected on a routine basis, are collected only for selected points, and are prone to measurement errors and inconsistencies, especially where multiple mine staff are involved in its collection. The resulting variability in mine geodetic data has the potential to trigger false alarms or give misleading trends. For example, the geodetic data for the ventilation shaft indicates caving-induced movements as shown in Fig. 17 but with significant variability of ± 60 mm. In the meantime, the InSAR measurements (and the FLAC3D prediction) for the ventilation shaft do not oscillate to the same degree around the mean trend. These observations emphasise the significant value of the InSAR data and thus the InSAR calibrated FLAC3D model regarding subsidence prediction.

6. Conclusions

This study presents results from a detailed 3-D back and forward analysis of caving-induced displacements at the Palabora open pit/block cave mine in South Africa. Results from the back analysis of a 2005 pit slope failure were used to constrain uncertainty in the rock mass properties and far-field in-situ stresses, as well as to bring understanding to the problem with respect to the cave–pit interactions. The modelled outcome underscores the sensitivity and dependence of numerical results on the input required and thus the difficulty of using modelling results for predictive purposes. Agreement was found between the FLAC3D modelled zones of ground movement and the location of the 2005 northwest wall pit slope failure, as well as with RADARSAT-1 InSAR data from 2005.

A "best fit" set of input properties were obtained and used for forward modelling of the caving-induced subsidence occurring at Palabora for the period 2009–2010. Dedicated high-resolution InSAR data from the recently launched RADARSAT-2 satellite was collected for the same period (March 2009–March 2010). Again, close agreement was achieved with respect to the spatial extent and magnitudes of the FLAC3D predicted displacements and those measured using InSAR, allowing further calibration of the model. These were further compared with geodetic monitoring data from the mine likewise showing very good agreement.

The close fit achieved between the predictive 3-D numerical model and InSAR data demonstrates the promise of InSAR as a means to calibrate and validate sophisticated numerical models, and thereby contribute to the management of block caving associated subsidence hazards. The results demonstrate that satellite-based InSAR provides an effective means to identify and map spatial movements across a large open pit and beyond the pit limits. This ability is important for protecting key mine infrastructure. For an existing mine, such as Palabora, the InSAR-calibrated model represents a means to give an advanced warning of any potential subsidence threats or those related to unfavourable interactions between the advancing cave and overlying pit slopes. For a Greenfield site, the same degree of model calibration may not be possible but modelling could still play a key role in safely locating critical infrastructure.

Together, an advanced information product has been developed and demonstrated, integrating geology, geotechnical data sets, and 3-D numerical modelling with InSAR imagery to assist mining decision makers in their development of safe and efficient block caving and open pit mining operations.

Acknowledgements

This work was funded through a grant from the Canadian Space Agency (contract#: F028-07-1686) and a Collaborative Research and Development grant from the Natural Science and Engineering Research Council of Canada (NSERC) in partnership with Rio Tinto. The authors would like to thank Rio Tinto and the Palabora mine staff for providing data, Dr. Andre van As (Rio Tinto Technical Services), Guy Aube (Canadian Space Agency) and Christian Nadeau (MDA Systems) for their technical guidance, and Jordan Severin (University of British Columbia) and Dr. Tom Styles (AMC Mining Consultants UK Ltd.) for their assistance in developing the cave geometries.

References

[1] Laubscher D. A practical guide manual on block caving. Prepared for the international caving study (ICS 1997–2000); 2000.
[2] Karzulovic A, Cavieres P, Pardo C. Caving subsidence at El Teniente mine. 1999. [in Spanish].
[3] Gilbride LJ. Free KS, Kehrman R. Modeling block cave subsidence at the Molycorp, Inc., Questa Mine. 2005. Paper 05–881.
[4] Brummer R, Li H, Moss A. The transition from open pit to underground mining: an unusual slope failure mechanism at Palabora. 2006; p. 411–20.
[5] Beck D, Pfitzner M. Interaction between deep block caves and existing, overlying caves or large open pits. 2008; p. 381–91.
[6] Sainsbury BL, Pierce M, Mas Ivars D Simulation of rock-mass strength anisotropy and scale effects using a ubiquitous-joint rock mass (UJRM) model. 2008; Paper 06-02: p. 241–50.
[7] Vyazmensky A. Numerical modelling of surface subsidence associated with block cave mining using a finite element/discrete element approach. PhD thesis. Burnaby (British Columbia): Simon Fraser University; 2008.
[8] Vyazmensky A, Stead D, Elmo D, Moss A. Numerical analysis of block caving-induced instability in large open pit slopes: A finite element/discrete element approach. Rock Mech Rock Eng 2010;43:21–39.
[9] Moss A, Diachenko S, Townsend P. Interaction between the block cave and the pit slopes at Palabora mine. J S Afr Inst Min Metall 2006;106:479–84.
[10] Palabora Mining Company Limited. Mine geological and mineralogical staff. The geology and the economic deposits of copper, iron, and vermiculite in the Palabora igneous complex: a brief review. Econ Geol 1976;71(1):177–92.
[11] Piteau Associate Engineering LTD. Assessment of pit wall instability and slope displacement as a result of interaction between the pit and underground mine. Report to Rio Tinto Management Services SA (Pty) Ltd; January 2005.
[12] Itasca Consulting Group. FLAC3D—Fast Lagrangian analysis of continua in 3 dimensions, version 4.0. Minneapolis: Itasca Consulting Group, Inc.; 2009.
[13] Hoek E, Carranza-Torres CT, Corkum B. Hoek–Brown failure criterion—2002 edition. 2002; p. 267–73.
[14] Hoek E. Practical rock engineering. Toronto: Rocscience, e-book; 2007.
[15] Heidbach O, Tingay M, Barth A, Reinecker J, Kurfeß D, Müller B. The world stress map database release 2008. http://dx.doi.org/10.1594/GFZ.WSM.Rel2008; 2008.
[16] Stacey TR, Wesseloo J. In situ stresses in mining areas in South Africa. J S Afr Inst Min Metall 1998;98(7):365–8.
[17] SRK Consulting Group. Measurement of in situ stresses at Palabora mine. Report to Rio Tinto Management Services SA (Pty) Ltd. 179447/2; 1992.
[18] SRK Consulting Group. Measurement of in situ stresses at Palabora mine. Report to Rio Tinto Management Services SA (Pty) Ltd. 179447/5; 1992.
[19] Gash, P. Analysis and interpretation of the in situ stress measurement carried out in raw#1 on the production level; 1999.
[20] Martin DC, Newcomen HW. Palabora Mining Company, Phalaborwa, South Africa, copper open pit 1991 geotechnical studies, geotechnical assessments and numerical modelling for the west wall. Piteau Associates, Report to Palabora Mining Company. 91-686J; August 1991.
[21] SRK Consulting Group. Palabora underground mine pre-feasibility study, 1. Report to Rio Tinto Management Services SA (Pty) Ltd. 179447; 1991.
[22] National Coal Board. Subsidence engineers handbook. 2nd edn. London: Coal Board Mining Department; 1975.
[23] Zebker HA, Rosen PA. On the derivation of coseismic displacement fields using differential radar interferometry: the Landers earthquake. J Geophys Res 1994;99(B10):19,617–9.
[24] Rabus B, Eberhardt E, Stead D, Ghuman P, Nadeau C, Woo K, et al. Application of InSAR to constrain 3-D numerical modelling of complex discontinuous pit slope deformations. 2009.